Supplementary Information for

Flexible and Robust Te/PET Films for Ultrafast All-Optical Terahertz Modulators

Pujing Zhang[1,2,#], Donggang Xie[3,#], Longyu Shi[1], Haojing Wang[4], Guangwei She[4], Wensheng Shi[4], Peijie Wang[1], Cunlin Zhang[1], Kuijuan Jin[3], Chen Ge[3,*], and Qingli Zhou[1,*]

[1] Key Laboratory of Terahertz Optoelectronics, Ministry of Education, and Beijing Advanced Innovation Center for Imaging Theory and Technology, Department of Physics, Capital Normal University, Beijing 100048, China

[2] Department of Electrical and Computer Engineering, National University of Singapore, Singapore 117583, Singapore

[3] Beijing National Laboratory for Condensed Matter Physics, Institute of Physics, Chinese Academy of Sciences, Beijing 100190, China

[4] Key Laboratory of Photochemical Conversion and Optoelectronic Materials, Technical Institute of Physics and Chemistry, Chinese Academy of Sciences, Beijing 100190, China

*gechen@iphy.ac.cn

*qlzhou@cnu.edu.cn

1. Transmission spectra of Te nanofilms

The transmission spectra shown in Figure S1 were obtained using an Optical pump-THz probe (OPTP) system. The measurement is taken by using a Ti: sapphire regenerative amplifier delivering ultrashort optical pulses with a duration of 100 fs and a central wavelength of 800 nm at a repetition rate of 1 kHz. The source beam is split into three portions, corresponding to THz generation, probe, and pump beams, respectively. The path with THz radiation is enclosed and purged with dry nitrogen. The power of pump beam with 0.3 cm^2 spot size is variable. We first measured the transmitted THz time-domain signals of PET substrate ($E_{sub}(t)$) and Te/PET films ($E_{sam}(t)$) by blocking the pump beam, as shown in Figure S1a. Then, a one-dimensional pump curve of sample can be recorded by scanning the pump delay line with the fixed position of THz generation delay line at the peak of the THz pulse. The transmitted THz time-domain signals of Te/PET films under different pump powers were obtained by regulating the pump beam at a specific pump time delay corresponding to the maximum modulation. These time-domain signals were transformed into the frequency domain through a fast Fourier transformation, giving the frequency-dependent amplitude ($T_{sub}(\omega)$ and $T_{sam}(\omega)$). The transmission spectra plotted in Figure S1b were calculated by $T(\omega)= T_{sam}(\omega)/T_{sub}(\omega)$. The transmission spectra of Te nanofilms at pump delay time of 0 ps exhibit the power-dependent but frequency-independent broadband features. It is worth noting that this material has a high transmission of about 96.1% without pump, leading a very low insertion loss of -0.35 dB calculated by 20lg (E_{sam}/E_{sub}), where E_{sam} and E_{sub} are the THz amplitudes for sample and substrate, respectively. With increasing pump power, the transmission exhibits a monotonic decrease across the broadband frequency range of 0.4-2.2 THz.

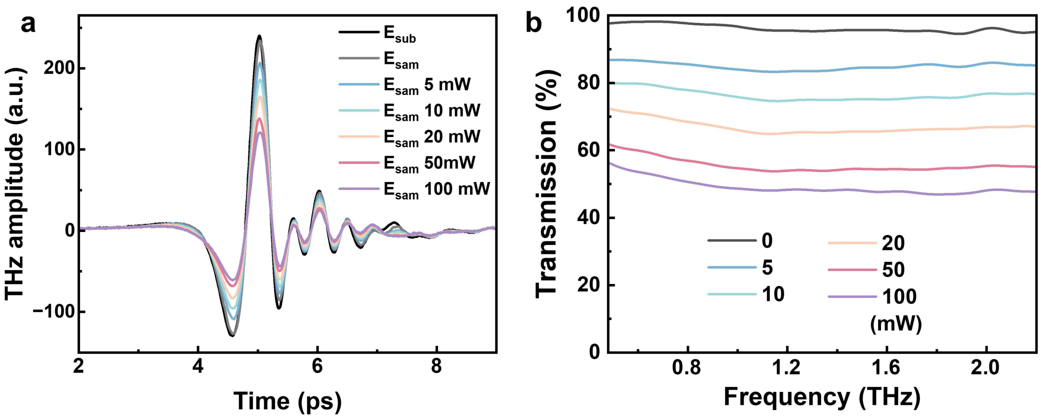

Figure S1. a THz time-domain signals and **b** transmission spectra of Te/PET films under different pump power at pump delay time of 0 ps.

Table S1. Comparison of reported device properties based on flexible THz modulators

Device materials	Modulation method	Modulation depth	Pump conditions	Photocarrier lifetimes
VO_2/mica [1]	Mechanical/optical	40%	800 nm, 6.4 mJ/cm^2	~1 ms
$CH_3NH_3PbBr_3$ [2]	Mechanical/optical	30%	800 nm,16.7 mW/cm^2	——
$Ti_3C_2T_y$ [3]	Optical	3%	800 nm, 950 μJ/cm^2	560 ps
Ge/Kapton [4]	Optical	24%	800 nm, 1200 mW	9.5 ps
Gr/PET [5]	Mechanical	32%	——	——
Ge/COC [6]	Optical	5%	800 nm, 654 μJ/cm^2	6 ps
GST/PET [7]	Mechanical/optical	2.5%	800 nm, 500 mW	10 ps
2D perovskites [8]	Optical	2.5%	800 nm, 550 μJ/cm^2	9 ps
Te/PET **(this work)**	Mechanical/optical	50%	800 nm, 100 mW (260 μJ/ cm^2)	8.5 ps

2. Supplementary measurements for uniformity and stability of devices

As presented in Figure S2, we measured the transient THz photoresponse at 100 different spatial positions across the Te/PET sample under the pump power of 20 mW. The *MD*(*t*) curves derived from all locations exhibit the relatively concentrated distribution, reflecting excellent device uniformity. Furthermore, the corresponding statistical distribution histogram of *MD*(*t*=0) for the measured locations is well-fitted by a Gaussian distribution to confirm the consistency of the device performance.

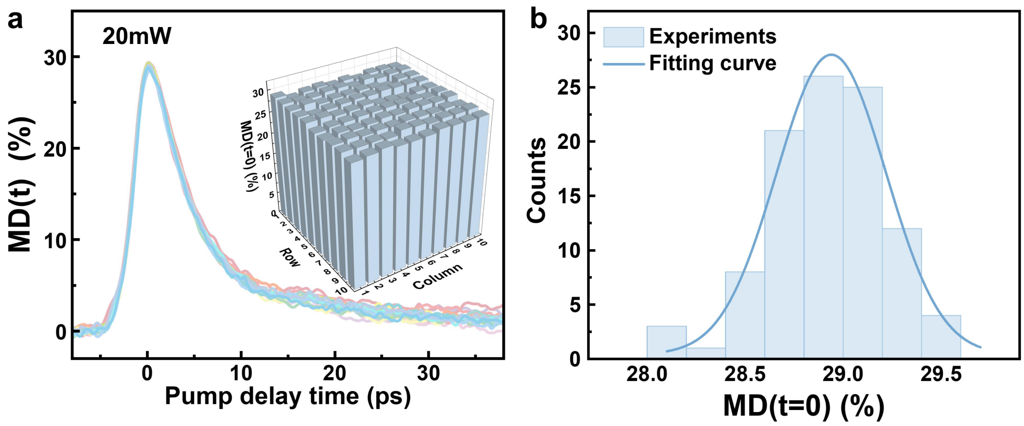

Figure S2. a *MD*(*t*) curves at 100 different spatial positions across Te/PET samples under pump power of 20 mW. Insets: *MD*(*t*=0) histogram of the devices. **b** Corresponding statistical diagram of *MD*(*t*=0). The fitting curve is a Gaussian function.

As shown in Figure S3, transient THz dynamics curves of Te/PET device are recorded after 7, 30, and 90 days under air exposure. The experimental results demonstrate that the device maintains highly consistent performance compared to its initial state, confirming that the Te-based flexible device possesses exceptional long-term stability to ensure the robustness for practical applications.

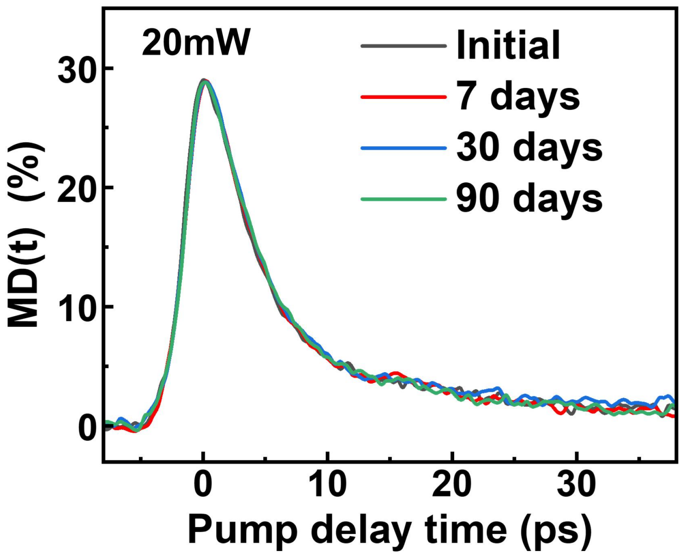

Figure S3. Transient THz dynamics curves of Te/PET samples after 7, 30 and 90 days under air exposure.

As shown in Figure S4, our measured results indicate that the modulation performance remains stable even after 10000 bending cycles at a bending radius of 6 mm. Those transient THz dynamics curves of Te/PET films do not exhibit obvious variation after various bending cycles (2000, 5000, 10000). This immunity to mechanical fatigue further confirms that the Te/PET device is an ideal candidate for practical applications.

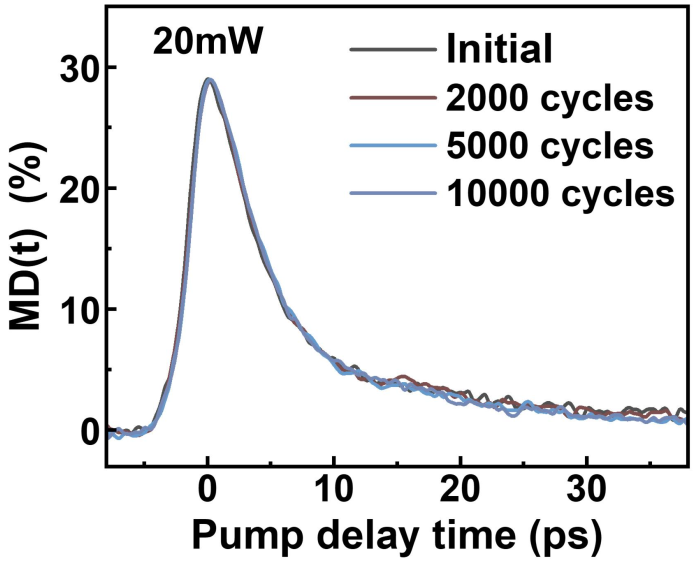

Figure S4. Transient THz dynamics curves of Te/PET samples under different numbers of bending cycles (2000, 5000, 10000) at a bending radius of 6 mm.

3. Raman spectra of Te/PET device under different bending cycles

We utilize the Raman spectra to investigate the effect of bending states on the lattice structure, as given in Fig. S5. The three characteristic vibration peaks exhibit no obvious shifts, indicating that the Te nanofilm maintains its high structural integrity and original crystalline state without significant lattice distortion during the bending process.

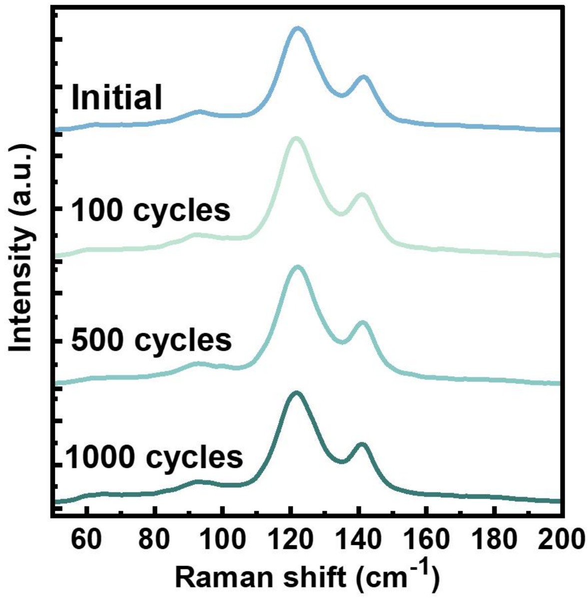

Figure S5. Raman spectra of Te/PET device under different bending cycles.

4. Confusion matrices under bending conditions

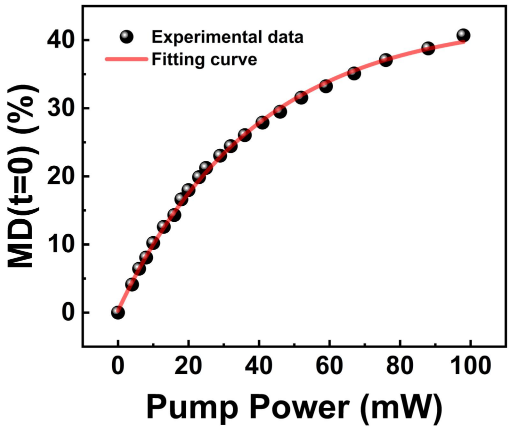

Figure S6. The mapping relationship between THz pump power and encoded *MD*.

Figure S7 shows the confusion matrices of the classification results of the 10,000 test images after 30 epochs under different bending conditions. The columns here designate the actual labels of stimuli images, while the rows represent the inferred results, and the color bars indicate the number of instances. It is evident that the confusion matrices under all tested bending radii and cycles exhibit negligible deviations from the initial state, characterized by dominant diagonal elements and sparse off-diagonal errors. The results verify that the mechanical robustness of the device effectively translates into high-performance pattern recognition.

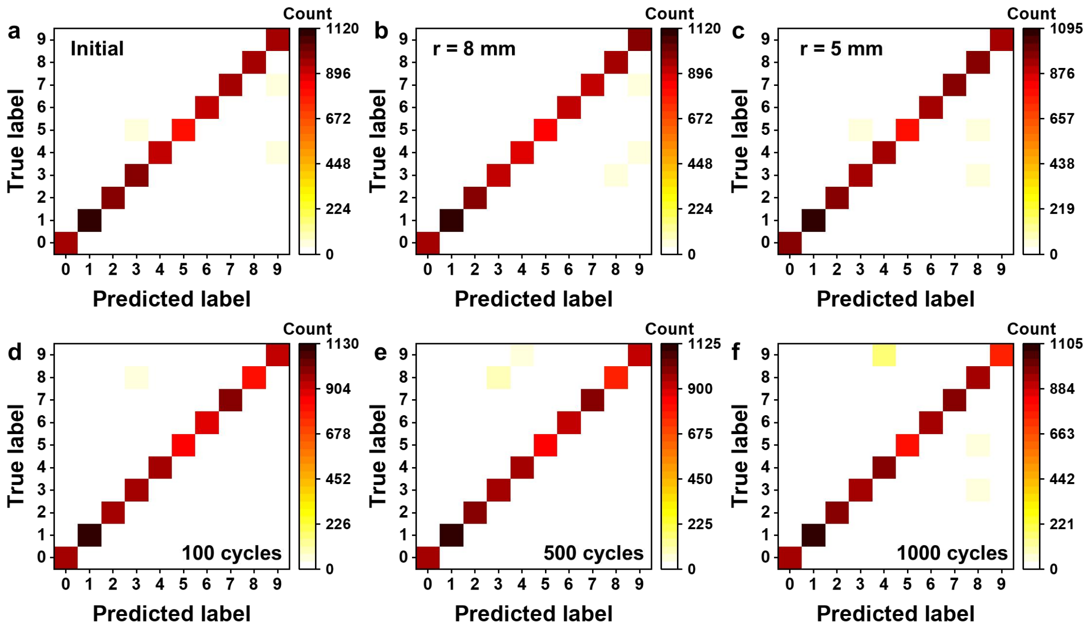

Figure S7. Confusion matrices of the classification results of the test dataset under different bending conditions.

References

S1. Chang, X. *et al*. Impact of the uniaxial strain on terahertz modulation characteristics in flexible epitaxial VO_2 film across the phase transition. *Optics Express* **31**, 13243 (2023).

S2. Fan, X. et al. Highly deformable and high-performance optical paper-based perovskite terahertz modulator. *Optics Express* **33**, 7978-7988 (2025).

S3. Li, G. *et al*. Dynamical control over terahertz electromagnetic interference shielding with 2D $Ti_3C_2T_y$ MXene by ultrafast optical pulses. *Nano Letters* **20,** 636-643 (2020).

S4. Lim, W. X. *et al*. Ultrafast all-optical switching of germanium-based flexible metaphotonic devices. *Advanced Materials* **30**, 1705331 (2018).

S5. Cheng, L. *et al*. Mechanical terahertz modulation based on single-layered graphene. *Advanced Optical Materials* **6**, 1700877 (2018).

S6. Wang, K. *et al*. Nanometric Ge films for ultrafast modulation of THz waves with flexible metasurface. *Advanced Optical Materials* **12**, 2402010 (2024).

S7. Pitchappa, P. *et al*. Volatile ultrafast switching at multilevel nonvolatile states of phase change material for active flexible terahertz metadevices. *Advanced Functional Materials* **31**, 2100200 (2021).

S8. Kumar, A. *et al*. Excitons in 2D perovskites for ultrafast terahertz photonic devices. *Science Advances* **6**, eaax8821 (2020).